Supplementary Information (SI) for RSC Advances.
This journal is © The Royal Society of Chemistry 2026

Supplementary Information for

Small buds to blooming flowers: Organic–inorganic hybrid nanoflowers as immobilization platform and robust system for bio-catalytic production of D-allose

Sweety Sharma[a,b], Shantanu B. Sathaye[a,c], Yeddula Nikhileshwar Reddy[a], Jayeeta Bhaumik[a], and Sudhir Pratap Singh, [a,c]*

[a]Center of Innovative and Applied Bioprocessing (BRIC-NABI), Sector 81, SAS Nagar, Mohali, India.

[b]Indian Institute of Science Education and Research, Mohali

[c]Department of Industrial Biotechnology, Gujarat Biotechnology University, GIFT City, Gandhinagar, Gujarat 382355, India.

*Corresponding authors' email: sudhir.singh@gbu.edu.in

Contents

1. Instrumentation

Data from Scanning electron microscopy (SEM, JSM-6000PLUS JEOL), Fourier Transform Infrared (FTIR) spectroscopy (Spectrum two, PerkinElmer), Dynamic light scattering particle analyzer (DLS, Malvern, USA), Powder X-Ray Diffraction (Rigaku), Brunauer-Emmett-Teller (BET) analyser (Anton Paar, ASiQ), Differential Scanning Calorimetry/Thermogravimetric analysis (DSC/TGA) (PerkinElmer STA 8000) UV-Visible spectrophotometer (UV-Vis, Shimadzu UV-2600), Lyophilyzer (Delta 2-24 LSC Plus Christ) were recorded at Center of Innovative and Applied Bioprocessing (CIAB), Mohali. Field emission Scanning electron microscope (FE-SEM, Apreo S HiVac, ThermoFisher Scientific), Transmission Electron Microscope (TEM, JOEL 1400) and Confocal Laser Scanning Microscopy (Zeiss LSM880) were recorded at National Agri-Food Biotechnology Institute (NABI), Mohali.

2. Experimental Section

2.1. Cloning, Expression and Purification of Recombinant Enzyme

The construct was introduced in the expression host, *E. coli* BL21, for gene expression and production of His-tagged L-RI_M protein. The recombinant cells were cultured in Luria-Bertani (LB) medium containing 10 mg L^{-1} kanamycin as a selection marker, then diluted in 200 ml LB with kanamycin at 37 ^oC/200 RPM to achieve 0.6 OD_{600}. Gene expression was induced by 0.5 mM isopropylthio-β-galactoside (IPTG), followed by cell culture at 16 ^oC /150 RPM for 16-20 h. The culture was harvested by centrifugation at 4 ^oC/6000 RPM for 5 min. The cell pellet was washed with 0.85% saline water and re-suspended in lysis buffer (50 mM HEPES [pH 7.0] and 300 mM NaCl). The cells were sonicated for 3 minutes (3s pulse on and 10s off) at an amplitude of 30 (Q Sonica, USA) to disrupt cells, releasing proteins into the buffer. The lysate was centrifuged at 4 ^oC/10,000 RPM for 45 min to pellet the cellular debris. The crude cell extract was subjected to affinity chromatography in Nickel-Nitrilotriacetic acid (Ni-NTA)

matrix column (Qiagen) for separation and purification of His-tagged L-RI_M protein. The Ni-NTA column was equilibrated with the equilibrium buffer (50 mM HEPES buffer [pH 7.0], 300 mM NaCl and 10 mM Imidazole). The crude cell extract was then passed through pre-equilibrated Ni-NTA column. The column was washed with wash buffer (50 mM HEPES buffer [pH 7.0], 300 mM NaCl and 40 mM Imidazole), and finally, His-tagged L-RI_M protein was eluted in 500 µl aliquots by using elution buffer (50 mM HEPES buffer [pH 7.0], 300 mM NaCl and 300 mM Imidazole). The protein purification was performed in AKTA pure protein purification system at 4 °C. This was followed by membrane dialysis to remove salt and imidazole. The concentrated purified protein fraction of L-RI_M was obtained by using an amicon filter (cut off 30 kDa, Merck) and checked on SDS-PAGE (**Figure S1**). The protein concentration was determined by Bradford assay using Bradford reagent (Sigma-Aldrich, St. Louis, Missouri) with bovine serum albumin (BSA) as a standard.

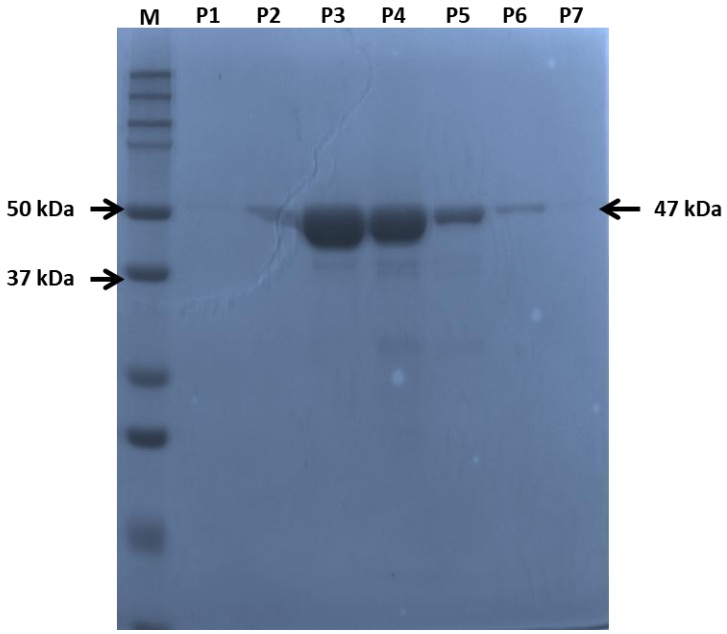

Figure S1. SDS-PAGE of purified L-RI_M. M- Marker; P1-Purified fraction 1; P2-Purified fraction 2; P3-Purified fraction 3; P4-Purified fraction 4; P5-Purified fraction 5; P6-Purified fraction 6 and P7-Purified fraction 7.

2.2. Preparation of L-Rhamnose isomerase Manganese-Nanoflowers (L-RI_{Mn}NFs)

2.2.1. Effect of different enzyme concentrations on L-RI_{Mn}NFs. To observe the effect of different enzyme concentrations on the morphology, NFs were synthesized by using varying amounts of purified L-RI_M (0.05 mg ml^{-1} to 0.5 mg ml^{-1}).

2.2.2. Effect of different metal salt concentrations on L-RI_{Mn}NFs. To observe the effect of different metal salt concentration, NFs were synthesized in the presence of 0.5 to 5mM concentration.

2.2.3. Effect of different incubation period on L-RI_{Mn}NFs. The change in the morphology of nanoflowers at different time periods was observed by incubating the NFs' synthesizing components for different time periods (0 h to 84 h).

2.2.4. Effects of Trypsin and EDTA on L-RI_{Mn}NFs. To see the effect of the degradation of organic component of the organic-inorganic assembly, freshly synthesized L-RI_{Mn}NFs were treated with trypsin. NFs were also treated with the metal chelating agent EDTA, to observe the effect of the absence of inorganic component on these self-assembled structures.

2.3. Quantification of L-RI_M on L-RI_{Mn}NFs

The initial enzyme concentration (0.2mg/ml), enzyme concentration after loading and the enzyme in supernatant/washout was measured from absorbance at 280nm following Beer-Lambert's law:

$A = \varepsilon cl$

Where, A is absorbance at 280nm, ε is the extinction coefficient for L-rhamnose isomerase enzyme (obtained through ProtParam, 67,380 $M^{-1}cm^{-1}$), c is the concentration and l is the path length (1 cm). So, the protein loading was calculated as below:

Method 1: c_{mol}= A of synthesised NFs/ $\varepsilon * l = 0.22/67{,}380 * 1 = 3.26 * 10^{-6}$ mol/L

$c_{mg/ml}$= 3.26*10^{-6}mol/L*47,000Da= 0.153mg/ml

Method 2: c= (Initial A-A in supernantant)/ ε*l

c_{mol}=(0.287-0.063)/67,380*1=3.32*10^{-6}mol/L

$c_{mg/ml}$= 3.32*10^{-6}mol/L*47,000Da= 0.156mg/ml

So, the enzyme loaded onto prepared NFs,

Loading yield= 0.156/0.2*100=78%

The concentration was also measured by using Bradford assay, following macro-assay (0.1 to 0.9mg/ml) and micro-assay (1 to 9µg/ml) for concentration of initial enzyme, loaded enzyme and enzyme in the supernatant/washout. The standard plots were prepared by using Bovine Serum Albumin (BSA) as standards and absorbance was measured at 595nm. **(Figure S2)** The loading yield was calculated using equation from standard graph which was close to 80%.

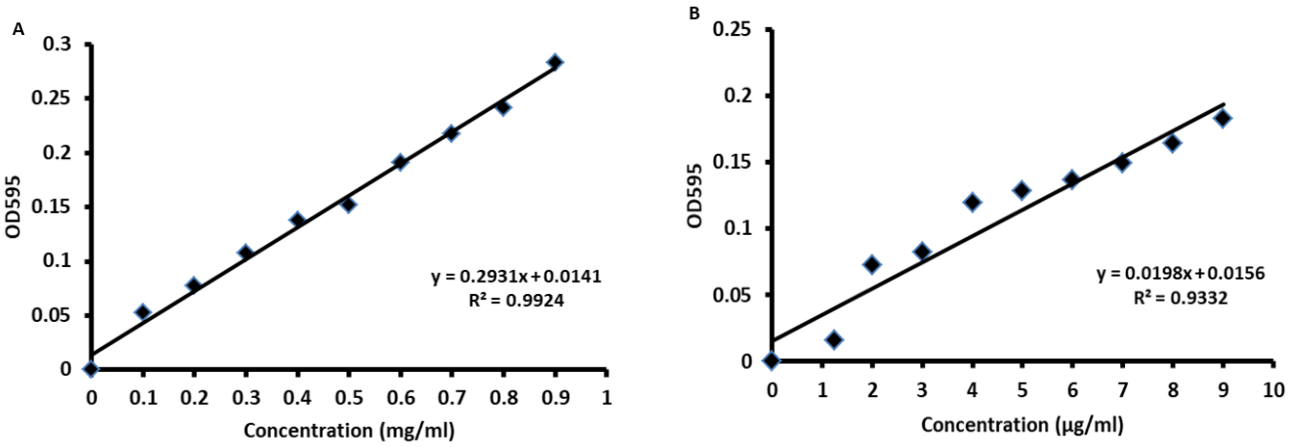

Figure S2. Standard curves of BSA using Bradford assay. (A) Macro-assay (concentration range 0.1 to 0.9mg/ml) and (B) Micro-assay (concentration range 1 to 9µg/ml)

2.4. Synthesis of L-RI$_{Mn}$NFs

The effect of different enzyme concentrations (0.05 to 0.5 mg/ml) was also examined on the synthesis of NFs (**figure S3**). In the case of low enzyme concentration (0.05 mg/ml), improper or incomplete flower morphology was observed. Increase in enzyme concentration (0.1 to 0.2 mg/ml), led to formation of flower-like structures. Further increase in the enzyme concentration caused increase in the thickness of the petals of nanoflower, with the decrease in the activity, which could be due to decrease in the surface area of the NFs and decreased porosity. Similar studies on lipase/$Cu_3(PO_4)_2$ NFs showed best morphology at 0.3mg/ml of enzyme concentration among 0.1 to 0.5 mg/ml. While the Trypsin/$Zn_3(PO_4)_2$ NFs exhibited most prominent structure at 0.05g among 0.025, 0.05 and 0.1g of trypsin. In case of co-immobilized NFs also, the enzyme concentrations and their ratios influence the morphology and activity of the immobilized enzymes.[1–3]

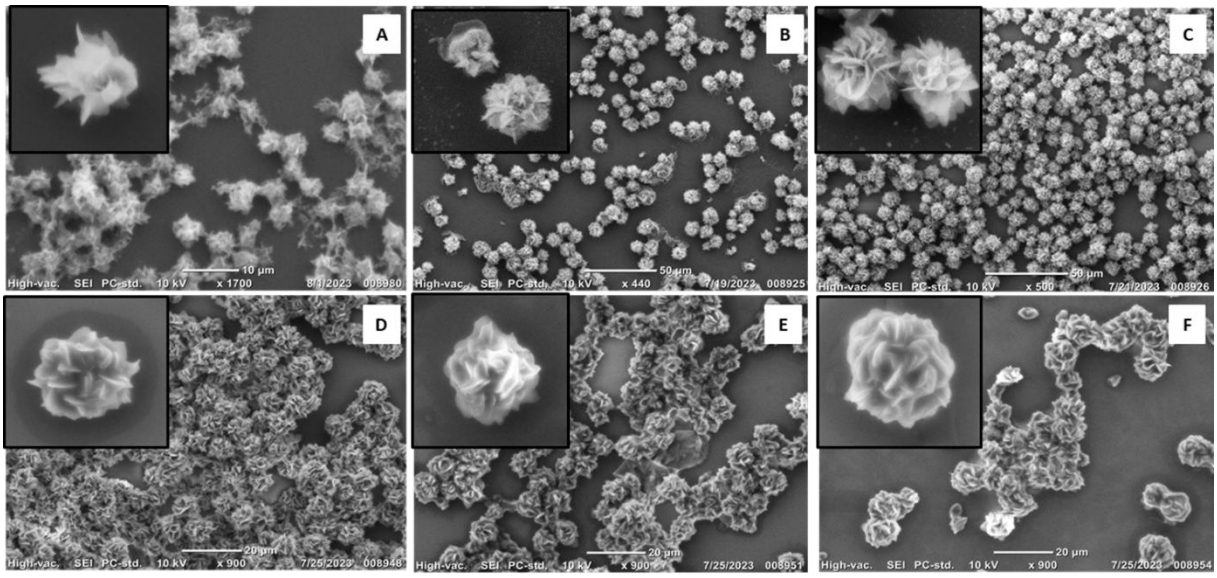

Figure S3. Effect of different enzyme concentrations on nanoflower morphology. A. 0.05 mg/ml, B. 0.1 mg/ml, C. 0.2 mg/ml, D. 0.3 mg/ml, E. 0.4 mg/ml, F. 0.5 mg/ml.

To understand the growth mechanism of the nano-assemblies, NFs were examined at different incubation periods (0, 12, 24, 48, 72 and 86 h). At early growth stages, the primary crystals of metal and phosphate are formed (**figure S4**). The results were relevant with previous studies which show that these layers form coordination bonds with the protein component of the mixture, and subsequently nanopetals appear.[4,5] As the incubation period increased, the nanopetals grew laterally to attain certain length and after about 48 h, the petals aggregated in epitaxial arrangement to form the fine and uniform flower-like morphology. The size range of nanoflowers was 7-9 µm in diameter. However, an incubation period of 72 h or more caused uncontrolled growth and agglomeration of the nanoflowers, leading to aggregation of the NF assemblies.

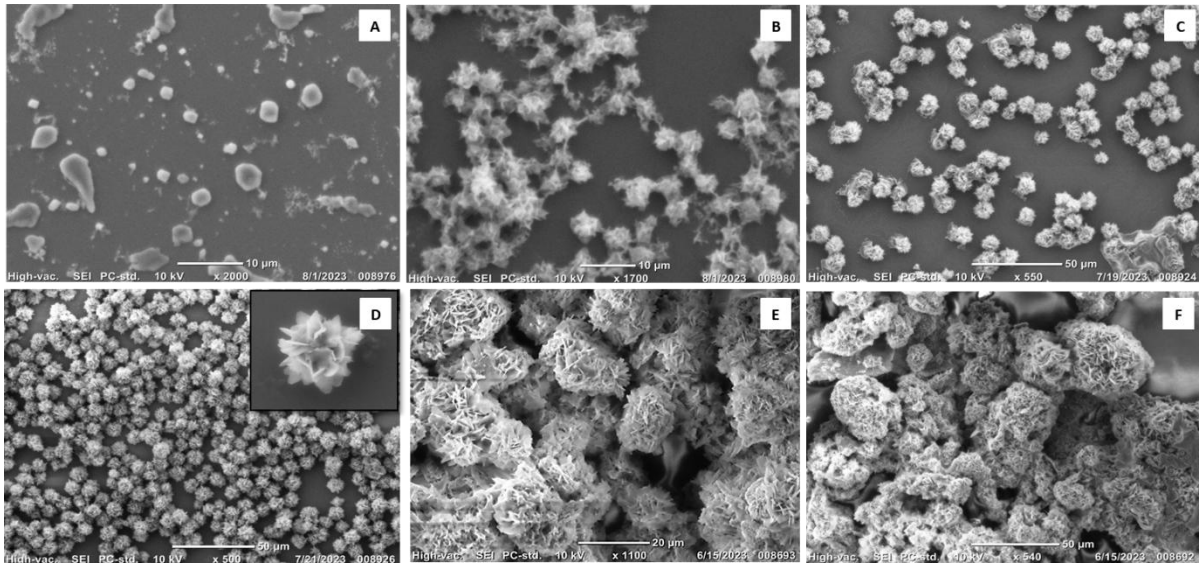

Figure S4. Morphology of nanoflowers after different incubation periods. A. 0 h, B. 12 h, C. 24 h, D. 48 h, E. 72 h, F. 86 h

The incubation temperature (e.g., 25 ℃ and 4 ℃) also affected the crystal's growth to some extent. (**Figure 2A** and **B**) At both the temperatures, the particle size was observed to be uniform, but the number of nanopetals and their thickness decreased at room temperature, as compared to 4 ℃ incubation. Though there was no significant difference in the activity, 4 ℃ incubation temperature was chosen for the synthesis of the NFs. The more compact structure

formed at 4 °C is probably the influence of slower aggregation of nanopetals facilitating more specific interactions. Also, lower temperature can prevent the proteolytic or other side reactions which could potentially hamper the process of aggregation. Duan et al. reported very low loading of carbonic anhydrase on to NFs mentioning the importance of optimizing temperature and other factors for NF synthesis. However, some studies suggest no difference in the catalytic activity when assembles at 4 °C/ 25 °C. For instance, N-acylhomoserine lactonase-based NFs showed no significant difference on activity either prepared at 4 °C or 25 °C.[3,6]

2.5. MD Simulation Section

Table S1: Molecular dynamic simulation system designing and system composition

System name	**Component**	**Temperature (°C)**
Control_4	*Protein+ **solvent	4
Control_25	*Protein+ **solvent	25
Test_4	*Protein+Mn^{2+}+ PO_4^{2-}+ **solvent	4
Test_25	*Protein+Mn^{2+}+ PO_4^{2-}+ **solvent	25

***Protein: L-RIM **Solvent: Water**

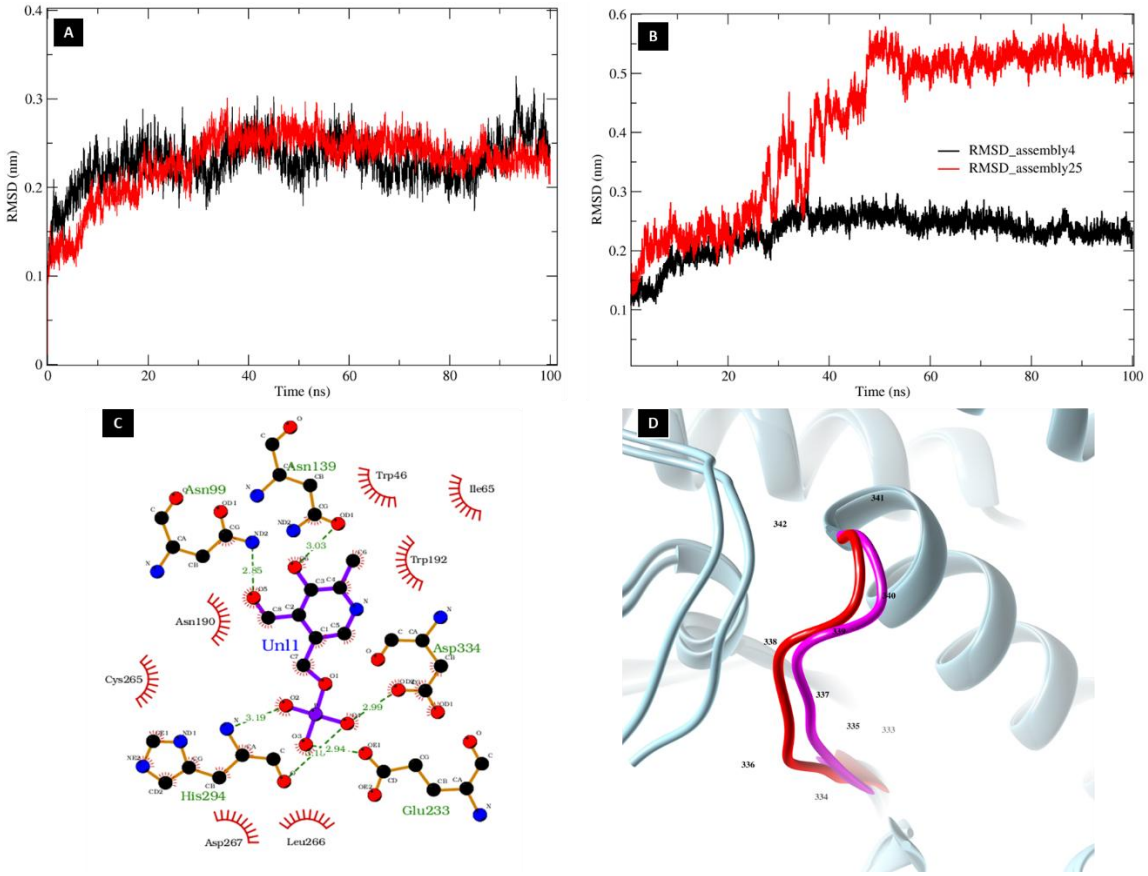

Figure S5. RMSD trajectory analysis. (A) Test_4 (avg. value 0.23 ±0.03 nm) and control_4 (avg. value 0.229 ±0.026 nm), (B) comparison between RMSD values between Test_4 and Test_25, (C) Interaction between D-allulose (substrate; Unl1) with the Active site residues of the L-RIM protein of Test_4, (D) Comparison of the conformations of α-β loop of the Test_4 (yellow) and control_4 (orange) systems.

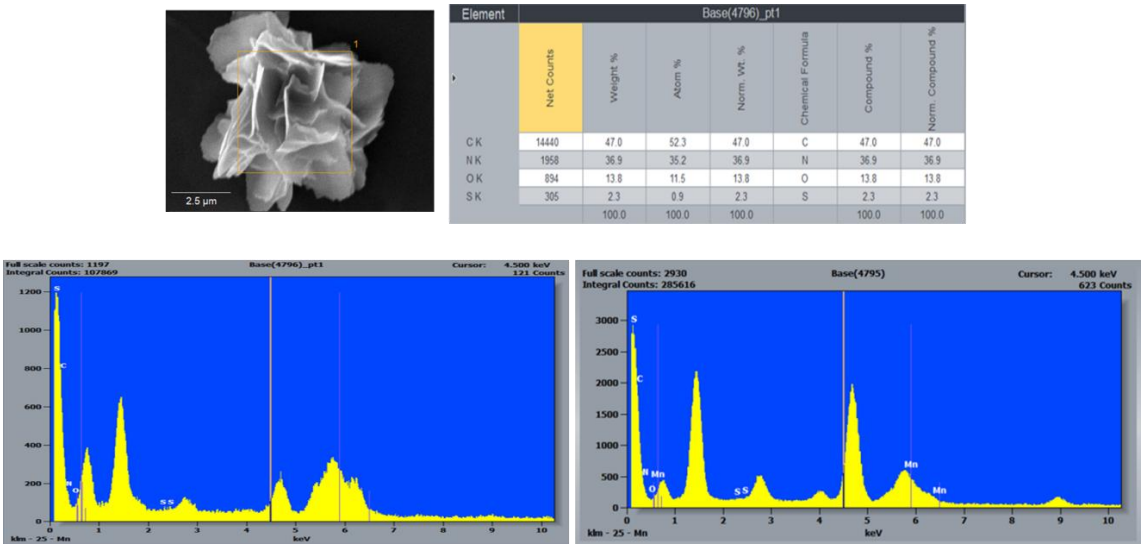

Figure S6. EDX element detection and distribution.

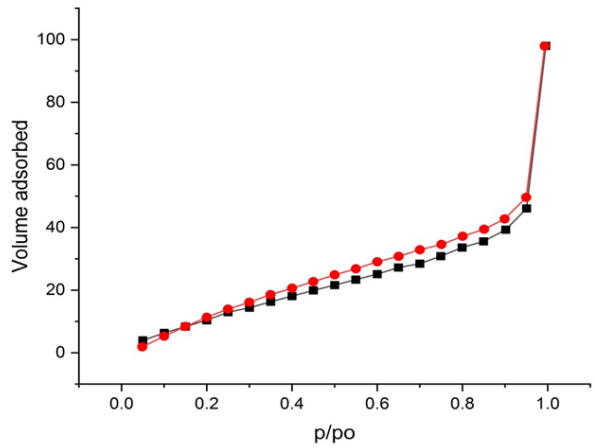

Figure S7. BET isotherm of lyophilized L-RI_{Mn}Nfs

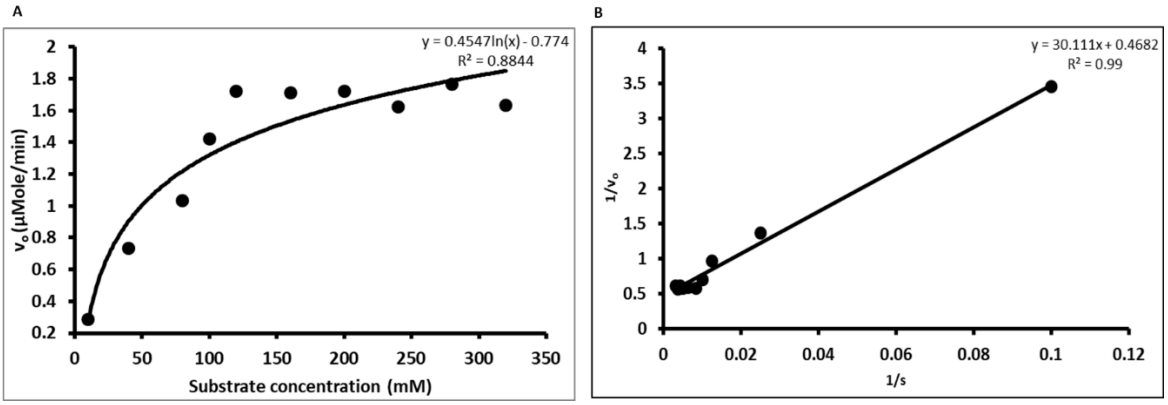

Figure S8. (A) Michelis-Menton kinetics of D-allose synthesis by L-RI_{Mn}Nfs and (B) Lineweaver-Burk plot.

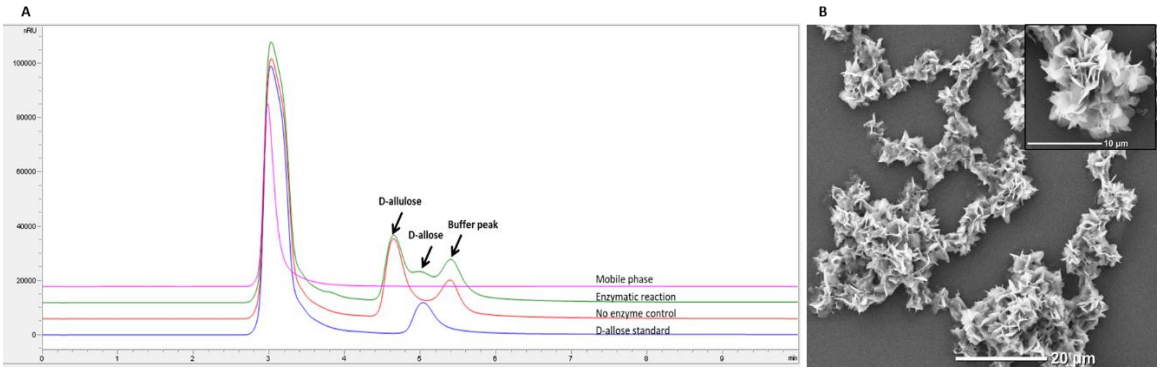

Figure S9. (A) Chromatograms showing D-allose synthesis, and (B) SEM image of L-RI_{Mn}Nfs after 6 cycles of reuse.

Table S2: Comparative catalytic parameters of immobilized L-rhamnose isomerases.

Immobilization matrix	**Type of interaction**	**Conversion (%)**	**k_{cat} (s^{-1})**	**K_m (mM)**	**k_{cat}/K_m ($mM^{-1}\ s^{-1}$)**	**References**
Chitopearl beads BCW 2603	Adsorption	NR	NR	NR	NR	[7]
Chitopearl beads BCW 2510	Adsorption	25	NR	NR	NR	[8]
BCW-2510 Chitopearl beads	Adsorption	30	NR	NR	NR	[9]
Cross-linked enzyme aggregates (CLEA)	Cross-linking	25	NR	NR	NR	[10]
Amino Resin LX-1000EA	Cross-linking	36	NR	NR	NR	[11]
DIAION HPA25L resin	Adsorption	30.9	937.95	18.5	50.7	[12]
Manganese-Nanoflower (MnNfs)	Self-assembly (coordination bonds)	47	679.9	64.44	10.55	This study

NR: Not Reported

3. References

1 Z. Wang, P. Liu, Z. Fang and H. Jiang, *Int J Mol Sci*, 2022, **23**, 11853.

2 S. Anboo, S. Y. Lau, J. Kansedo, P. S. Yap, T. Hadibarata and A. H. Kamaruddin, *Heliyon*, 2024, **10**, e27348.

3 L. Duan, H. Li and Y. Zhang, *ACS Omega*, 2018, **3**, 18234–18241.

4 S. K. Rai, L. K. Narnoliya, R. S. Sangwan and S. K. Yadav, *ACS Sustain Chem Eng*, 2018, **6**, 6296–6304.

5 K. A. Al-maqdi, M. Bilal, A. Alzamly, H. M. N. Iqbal, I. Shah and S. S. Ashraf, *Nanomaterials 2021, Vol. 11, Page 1460*, 2021, **11**, 1460.

6 Y. Chen, P. Liu, J. Wu, W. Yan, S. Xie, X. Sun, B. C. Ye and X. Chu, *J Nanobiotechnology*, 2022, **20**, 1–15.

7 S. H. Bhuiyan, Y. Itami, Y. Rokui, T. Katayama and K. Izumori, *J Ferment Bioeng*, 1998, **85**, 539–541.

8 K. Leang, G. Takada, Y. Fukai, K. Morimoto, T. B. Granström and K. Izumori, *Biochimica et Biophysica Acta (BBA) - General Subjects*, 2004, **1674**, 68–77.

9 K. Morimoto, C. S. Park, M. Ozaki, K. Takeshita, T. Shimonishi, T. B. Granström, G. Takata, M. Tokuda and K. Izumori, *Enzyme Microb Technol*, 2006, **38**, 855–859.

10 B. T. Menavuvu, W. Poonperm, K. Leang, N. Noguchi, H. Okada, K. Morimoto, T. B. Granström, G. Takada and K. Izumori, *J Biosci Bioeng*, 2006, **101**, 340–345.

11 C. Li, L. Gao, K. Du, H. Lin, Y. Ren, J. Lin and J. Lin, *Bioprocess Biosyst Eng*, 2020, **43**, 645–653.

12 K. Morimoto, T. Suzuki, H. Ikeda, C. Nozaki and S. Goto, *J Gen Appl Microbiol*, 2022, **68**, 1–9.